Nanostructures

DOI: 10.1002/ange.200602383

Oxygen-Deficiency-Induced Superlattice Structures of Chromia Nanobelts**

Wei-Qiang Han, Lijun Wu, Aaron Stein, Yimei Zhu, James Misewich, and John Warren*

Nanostructures have attracted wide attention in recent years, because of their fascinating properties and promising technological applications. While nanowires can be used as elements for miniaturized electrical, fluidic, and optical devices, nanobelts can provide engineers with new building

[*] Dr. W.-Q. Han, Dr. L. J. Wu, Dr. Y. M. Zhu
Center for Functional Nanomaterials
Brookhaven National Laboratory
Upton, NY 11973 (USA)
Fax: (+1) 631-344-7370
E-mail: whan@bnl.gov
Dr. A. Stein, Dr. J. Warren
Instrumentation Division
Brookhaven National Laboratory
Upton, NY 11973 (USA)
Dr. J. Misewich
Condensed Matter Physics and Materials Science Department
Brookhaven National Laboratory
Upton, NY 11973 (USA)

[**] This work is supported by the U.S. DOE under contract DE-AC02-98CH10886.

materials for creating nanoscale sensors, waveguides, and lasers.[1–7] ZnO nanobelts with a rigid helical conformation were recently found to have a superlattice structure, which forms to reduce the electrostatic energy of the polar nanobelt surface.[7] Modulation structures have also been reported in other one-dimensional nano-objects, such as ZnSe nanowires,[8] ZnO:In nanowires,[9] and CdSe nanoribbons.[10]

The physical and chemical properties of transition-metal oxides can be changed dramatically by altering the oxidation state of the transition metal. In its different valence states, chromium forms various chromium oxides, such as CrO_3, Cr_2O_5, CrO_2, and Cr_2O_3. Chromium dioxide (CrO_2) is a half-metallic ferromagnet and, thus, has potential applications in magnetic-tunneling and spin-injection devices.[11,12] Chromia (Cr_2O_3) has been widely used as a green pigment, as a coating material for thermal protection and wear resistance, as a refractory material, and as a heterogeneous catalyst. Chromia is also an important insulating antiferromagnet, with a Néel temperature of 307 K, and is a suitable material for tunnel-junction barriers, both below and above the Néel temperature.[13] For antiferromagnetic nanomaterials, the number of surface spins increases as the particle size decreases. The uncompensated spins on the nanostructure surfaces may significantly affect the magnetic properties of the materials. Néel suggested that very fine particles of an antiferromagnetic material should exhibit particular magnetic properties, such as superparamagnetism or weak ferromagnetism.[14] Size and shape are two important factors affecting the properties of nanostructures.

Chromia nanoparticles and nanopores have been prepared by several methods, including sol–gel processes, microwave-plasma processes, sonochemical reactions, gas condensation, laser-induced pyrolysis, hydrazine reduction followed by thermal treatment, mechanochemical processing, urea-assisted homogeneous precipitation, and precipitation–gelation reactions.[15,16] Chromia whiskers with diameters of 2–10 μm were synthesized by heating a mixture of Cr_2O_3, Al_2O_3, SiO_2, and carbon powders in an electric furnace at 1400 °C.[17] Herein, we use a simple and efficient route to synthesize chromia nanobelts and nanorods: a piece of chromium is heated at 800 °C under an ethanol vapor flow. To our knowledge, this is the first report of chromia nanobelts and nanorods. Two new types of superlattice structures related to oxygen deficiency are also reported.

The synthesis of the chromia nanobelts and nanorods is as follows. First, we insert a chromium piece into a quartz tube inside a horizontal furnace. Argon is used as a protective gas during the heating stage. Once the temperature reaches 800 °C, ethanol vapor is introduced, while the temperature is kept at 800 °C for 1 hour. Next, we stop the heating and the flow of ethanol vapor, but maintain the flow of argon until the sample cools.

We first examined the shape and structure of the nanoparticles in the product by using scanning electron microscopy (SEM) and X-ray diffraction (XRD). To prepare the sample for transmission electron microscopy (TEM), we separated the nanobelts and nanorods from the substrate by supersonication in an alcohol solution, and then dispersed the solution containing the nanoparticles onto copper grids coated with lacy carbon. The TEM experiments were carried out with a high-resolution JEOL 3000F microscope equipped with a field-emission gun, at an accelerating voltage of 300 kV. Electron energy-loss spectroscopy (EELS) was performed using a Gatan energy-filter system.

In Figure 1, SEM images of the as-produced sample are shown. The sample consists mainly of nanobelts, but also contains some nanorods. The nanobelts have lengths of several micrometers, widths ranging from tens to hundreds of nanometers, and thicknesses ranging from a few nanometers to tens of nanometers. In general, the width and thickness of an individual nanobelt are quite uniform. Interestingly, nanobelts with thick bases and a fold along the belt axis are also observed in SEM images (Figure 1c), and confirmed by TEM images (Figure 1d). In the XRD patterns of the nanobelts and nanorods, most peaks can be indexed to rhombohedral Cr_2O_3 (JCPDS 38-1479: space group $R\bar{3}c$, $a = 0.495876$, $c = 1.35942$ nm), while the remaining peaks arise from the chromium substrate.

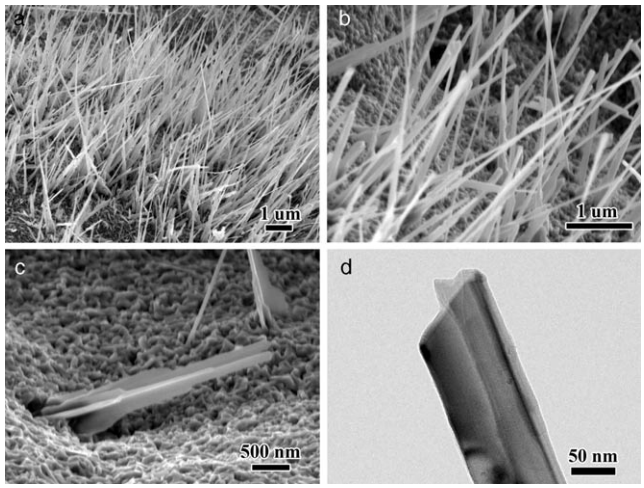

Figure 1. a), b) SEM images (at different magnifications) showing the growth of Cr_2O_{3-x} nanobelts and nanorods on the Cr substrate. c) SEM image and d) TEM image of nanobelts with a fold along the belt axis.

In Figure 2, a high-resolution TEM image along the [001] direction of a nanobelt and the corresponding selected-area electron diffraction (SAED) pattern are shown. Tilting experiments confirmed that the average structure of the nanobelts is rhombohedral with $a \approx 0.496$ and $c \approx 1.359$ nm. Actually, we found that many nanobelts are single-crystalline, with the surface normal of the largest faces being $\langle 001 \rangle$.

Figure 3a is a high-resolution TEM image along the $[\bar{1}11]$ direction of another nanobelt. The top-left part of the image shows the basic lattice fringes of the rhombohedral Cr_2O_3 structure, whereas the bottom-right part exhibits additional modulation fringes, as indicated by the arrows. Moiré effects can be ruled out, since no slightly mismatched or misorientated lattices are evident in the TEM image (Figure 3a), nor in the SAED pattern (Figure 3b). The diffraction pattern of the nanobelt exhibits satellite reflections indicating a structure modulation along the [110] direction (Figure 3b). The modulation wave vector is $q_1 = 1/3\,(a^* + b^*)$, and the perio-

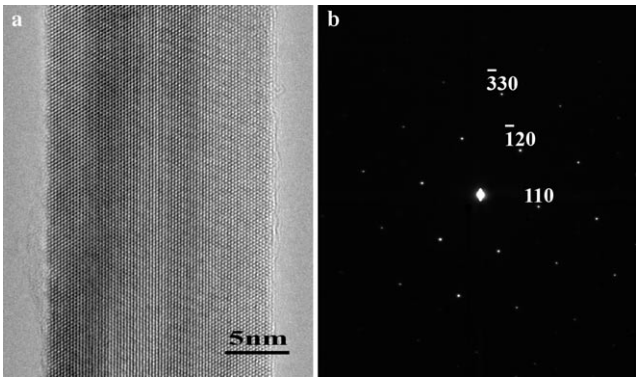

Figure 2. a) High-resolution TEM image and b) SAED pattern (along the [001] direction) of a Cr_2O_{3-x} nanobelt. Indexing refers to the cell of rhombohedral Cr_2O_3.

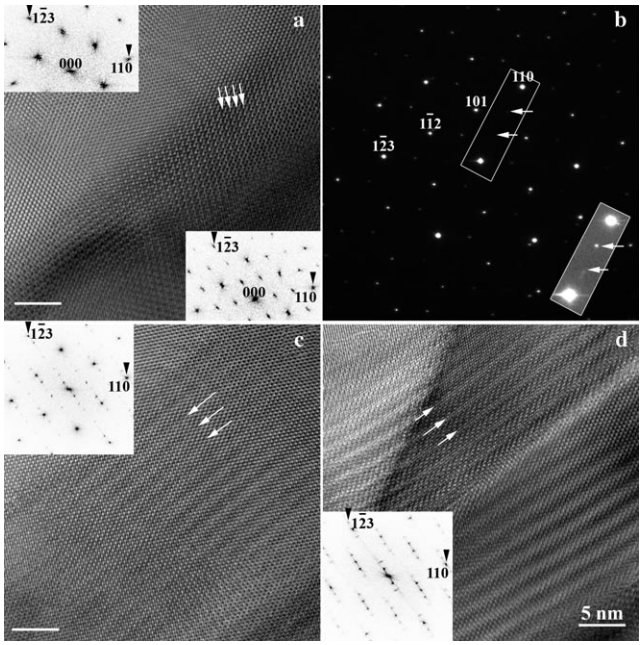

Figure 3. a) High-resolution TEM image (along the [$\bar{1}$11] direction) of a Cr_2O_{3-x} nanobelt with modulation I. No modulation of the basic rhombohedral Cr_2O_3 structure is observed in the top-left part of the image or in the corresponding Fourier transform (top-left inset). However, modulation I (arrows) is observed in the bottom-right part of the image and in the corresponding Fourier transform (bottom-right inset). b) SAED pattern (along the [$\bar{1}$11] direction) of the same nanobelt (from an area containing both unmodulated and modulated parts). Superlattice reflections (arrows) are enhanced in the inset. c) High-resolution TEM image (along the [$\bar{1}$11] direction) and corresponding Fourier transform (inset) of a nanobelt with modulation II at a periodicity of 1.64 nm (arrows). d) High-resolution TEM image (along the [$\bar{1}$11] direction) and corresponding Fourier transform (inset) of a nanobelt with modulation II at a periodicity of 1.84 nm (arrows). Indexing refers to the cell of rhombohedral Cr_2O_3. Scale bars = 5 nm.

dicity of the modulation in real space is 0.74 nm (hereafter, referred to as modulation I). Besides this commensurate modulation along the [110] direction, there is another incommensurate modulation approximately along the [$1\bar{2}3$]* (or [$0\bar{5}1$]) direction (hereafter, referred to as modulation II). The wave vector of the type-II modulation in Figure 3c is $q_2 \approx 0.133\,a^* - 0.267\,b^* + 0.401\,c^*$, and the periodicity in real space is 1.64 nm. The type-II modulation in Figure 3d is similar, but with a slightly longer periodicity of 1.84 nm in real space. Most of the nanobelts have structures with modulation II, but the periodicity of the modulation varies.

Electron energy-loss spectroscopy (EELS) can be used to analyze the chemical composition of TEM specimens, with a lateral resolution down to approximately 1 nm. To determine the origin of the modulation, we performed EELS analysis on the different types of nanobelts. In Figure 4a–c, EEL spectra

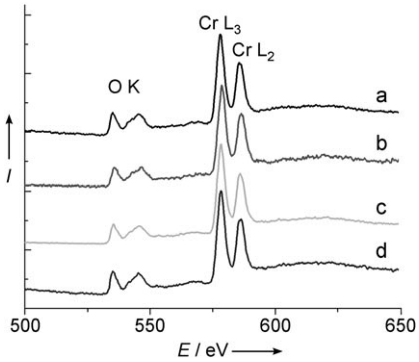

Figure 4. EEL spectra of Cr_2O_{3-x} nanobelts a) without modulation, b) with modulation I, and c) with modulation II, and of d) micron-sized Cr_2O_3 particles.

of chromia nanobelts without modulation, with modulation I, and with modulation II, respectively, are shown. For comparison, we also acquired a reference EEL spectrum (Figure 4d) of micron-sized Cr_2O_3 particles (Alfa–Aesar). The spectra were normalized to equalize the maximum intensities of the Cr L_3 peaks. Quantitative calculations show that the atomic ratio of oxygen to chromium in the nanobelts without modulation is $r_{O/Cr} = 1.47$ (Figure 4a), close to that of $r_{O/Cr} \approx 1.5$ in the micron-sized Cr_2O_3 particles. The $r_{O/Cr}$ of the nanobelts with modulations, however, is significantly lower: for those with modulation I, $r_{O/Cr} = 1.18$ (Figure 4b); for those with modulation II, $r_{O/Cr} = 1.22$ (Figure 4c). These ratios indicate an oxygen deficiency in the nanobelts with modulated structures. According to a series of EELS analyses, the composition of the nanobelts with modulations is Cr_2O_{3-x} with $x \approx 0.25$–0.70. Interestingly, many of the nanobelts with modulations have a composition near $Cr_2O_{2.4}$. No other elements were detected in the nanobelts by EELS (we examined the energy range of the C K edge in particular). TEM studies indicate that approximately 80% of the nanobelts have modulated structures.

The preparation of oxygen-deficient chromia, Cr_2O_{3-x}, as a powder was reported by Pop et al.[18] They first synthesized chromium hydroxide ($Cr(OH)_3$) gel by using CrO_3 and ethanol, and then heated the gel 1250 K in a hydrogen atmosphere. The XRD pattern of the product revealed that the nonstoichiometric product Cr_2O_{3-x} adopts the same structure as stoichiometric rhombohedral Cr_2O_3; only a slight difference in the peak positions and relative peak intensities was observed. Studies of X-ray K edge spectra by

Pop et al. further demonstrated that the composition of the nonstoichiometric Cr_2O_{3-x} is $Cr_2O_{2.4}$. As mentioned above, many of the nanobelts with modulations prepared by us also have a composition near $Cr_2O_{2.4}$, although their synthesis, morphology, and microstructure are completely different from those of the powder prepared by Pop et al. The oxygen vacancies in the nanobelts with modulations are ordered and are, thus, responsible for the observed superstructures.

The chemical reaction for the formation of the chromia nanobelts can be explained as: $4\,Cr + (3-x)\,O_2 \rightarrow 2\,Cr_2O_{3-x}$. The oxygen reactant mainly comes from the decomposition of ethanol at high temperatures (although we used argon (99.999%) to purge the reaction tube prior to heating, it may still have contained some remnant oxygen). The decomposition of ethanol not only supplies oxygen, but also carbon and hydrogen. Small amounts of carbon soot were found in the product by TEM. At high temperatures, chromium, like some other transition metals, such as tungsten,[19] is very easily oxidized, even at low oxygen concentrations. The presence of ethanol vapor ensures that chromium can be oxidized, but under oxygen-deficient conditions. To understand the role of ethanol in the synthesis, we tried replacing the ethanol vapor by water vapor or air, but in these cases, no nanobelts or nanorods were formed. Thus, ethanol plays an important role in the formation of the nanostructures. Further investigation of the formation mechanism will be carried out.

The Cr_2O_{3-x} nanobelts grow in an oxygen-deficient environment, which results in most of the nanobelts having an oxygen deficiency, as confirmed by the EELS measurements. The superstructures occur in the nanobelts containing oxygen defects (or vacancies), but not in those without oxygen defects. Thus, the modulations found in the oxygen-deficient nanobelts are due to the ordering of the oxygen vacancies. This hypothesis is also consistent with the XRD results, since X-ray scattering is not very sensitive to the light oxygen atoms.

The folded shape observed for some Cr_2O_{3-x} nanobelts is related to their crystal structure (Figure 1c,d). The structure of rhombohedral Cr_2O_3 is generally described by a hexagonal lattice with $a_H = 0.495876$ and $c_H = 1.35942$ nm (JCPDS 38-1479). However, it can be also described by a face-centered rhombohedral (fcr) lattice with $a_C = 0.7302$ nm and $\alpha = 85.546°$ according to Equations (1)–(3). The fcr lattice of

$$a_H = -1/2\,a_C + 1/2\,b_C \quad (1)$$

$$b_H = -1/2\,b_C + 1/2\,c_C \quad (2)$$

$$c_H = a_C + b_C + c_C \quad (3)$$

Cr_2O_3 deviates only slightly from a face-centered cubic (fcc) lattice ($\alpha = 90°$). In the fcc lattice, there are four equivalent axes with threefold symmetry ([111], $[\bar{1}11]$, $[1\bar{1}1]$, and $[11\bar{1}]$). For the fcr lattice, however, there is only one axis ($[001]_H$ or $[111]_C$) with true threefold symmetry. The other three ($[\bar{1}11]_C$, $[1\bar{1}1]_C$, and $[11\bar{1}]_C$) are pseudo-threefold axes. Since the deviation of the fcr lattice of Cr_2O_3 from an ideal fcc lattice is very small (4.454°), the differences between the true and the pseudo-threefold axes are also small. This situation often results in twin formation during crystal growth (for example, in $PrCo_2C_x$[20] and $YBa_2Cu_3O_{7-x}$ (YBCO)[21]). In Figure 5a, growth occurs along the $[111]_C$ direction in the left domain of

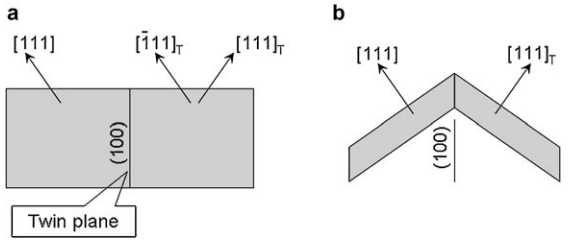

Figure 5. a) Formation of a (100) twin during bulk crystal growth. b) Formation of a folded nanobelt. Indexing refers to the fcr lattice; T subscripts refer to the second twin domain.

a bulk crystal, but along the $[\bar{1}11]_C$ direction in the right domain. The twin domains are related by the $(100)_C$ plane. As mentioned above, the Cr_2O_{3-x} nanobelts have the tendency to grow with their surface normals parallel to the $[001]_H$ (or $[111]_C$) direction. Thus, twinning across the $(100)_C$ plane results in the nanobelt folding shown in Figure 5b.

The oxygen-deficient chromia nanobelts with modulation structures and folded shapes described herein are expected to have distinct antiferromagnetic and catalytic properties.

Received: June 14, 2006
Revised: July 18, 2006
Published online: September 8, 2006

Keywords: chromium · nanostructures · oxides · superlattices · twinning

[1] Z. W. Pan, Z. R. Dai, Z. L. Wang, *Science* **2001**, *291*, 1647–1655.
[2] Z. L. Wang, *Annu. Rev. Phys. Chem.* **2004**, *55*, 159–196.
[3] M. Law, D. J. Sirbuly, J. C. Johnson, J. Goldberg, R. J. Saykally, P. D. Yang, *Science* **2004**, *305*, 1269–1273.
[4] H. Q. Yan, J. Johnson, M. Law, R. He, K. Knutsen, J. R. McKinney, J. Pham, R. Saykally, P. D. Yang, *Adv. Mater.* **2003**, *15*, 1907–1911.
[5] E. Comini, G. Faglia, G. Sberveglieri, Z. W. Pan, Z. L. Wang, *Appl. Phys. Lett.* **2002**, *81*, 1869–1871.
[6] W. Q. Han, L. J. Wu, Y. M. Zhu, M. Strongin, *Nano Lett.* **2005**, *5*, 1419–1422.
[7] P. X. Gao, Y. Ding, W. J. Mai, W. L. Hughes, C. S. Lao, Z. L. Wang, *Science* **2005**, *309*, 1700–1704.
[8] Q. Li, X. Gong, C. Wang, J. Wang, K. Ip, S. Hark, *Adv. Mater.* **2004**, *16*, 1436–1440.
[9] J. Jie, G. Wang, X. Han, J. G. Hou, *J. Phys. Chem. B* **2004**, *108*, 17027–17031.
[10] J. Joo, J. S. Son, S. G. Kwon, J. H. Yu, T. Hyeon, *J. Am. Chem. Soc.* **2006**, *128*, 5632–5633.
[11] K. P. Kamper, W. Schmitt, G. Guntherodt, R. J. Gambino, R. Ruf, *Phys. Rev. Lett.* **1987**, *59*, 2788–2791.
[12] G. A. Prinz, *Phys. Today* **1995**, *48*, 58–63.
[13] T. P. Kobylins, B. W. Taylors, *J. Catal.* **1973**, *31*, 450–458.
[14] L. Néel, *IEEE Trans. Magn.* **1981**, *17*, 2516.
[15] A. Kawabata, M. Yoshinaka, K. Hirota, O. Yamaguchi, *J. Am. Ceram. Soc.* **1995**, *78*, 2271–2273, and references therein.

[16] D. W. Kim, S. Shin, J. D. Lee, S. G. Oh, *Mater. Lett.* **2004**, *58*, 1894 – 1898.
[17] S. Hashimoto, A. Yamaguchi, *J. Mater. Sci.* **1996**, *31*, 317 – 322.
[18] I. Pop, M. Andrecut, I. Burda, C. Andrecut, O. Pop, I. Ivan, I. Nazarenco, C. Oprea, *Mater. Chem. Phys.* **1997**, *47*, 85 – 89.
[19] G. Gu, B. Zhang, W. Q. Han, S. Roth, J. Liu, *Nano Lett.* **2005**, *5*, 849 – 851.
[20] L. Wu, Y. Zhang, *Philos. Mag. A* **1997**, *76*, 481 – 492.
[21] Y. Zhu, M. Suenaga, J. Tafto, D. O. Welch, *Phys. Rev. B* **1991**, *44*, 2871 – 2874.

